How the Conical Intersection Seam Controls Regioselectivity in the Photocycloaddition of Ethylene and Benzene

Juan J. Serrano Pérez[a], Freija de Vleeschouwer[b], Frank de Proft[b], David Mendive-Tapia[a], Michael J. Bearpark[a], Michael A. Robb[a]

[a]Imperial College London, Department of Chemistry, Exhibition Road, London SW7 2AZ, United Kingdom, [b]Eenheid Algemene Chemie, Vrije Universiteit Brussel, Faculteit Wetenschappen, Pleinlaan 2, 1050 Brussels, Belgium.

Abstract

The photocycloaddition reaction of benzene with ethylene has been studied at the CASSCF level, including the characterization of an extended conical intersection seam. We show that the regioselectivity is, in part, controlled by this extended conical intersection seam and that the shape of the conical intersection seam can be understood in terms of simple VB arguments. Further, the shape and energetics of the asynchronous segment of the conical intersection seam, suggests that 1,2 (ortho) and 1,3 (meta) will be the preferred regioselectivities with similar weight. The 1,4 (para) point on the conical intersection is higher in energy and corresponds to a local maximum on the seam. VB analysis shows that the pairs of VB structures along this asynchronous seam are the same and thus the shape will be determined mainly by steric effects. Synchronous structures on the seam are higher in energy and belong to a different branch of the seam separated by a saddle point on the seam. On S_1 we have documented three mechanistic pathways corresponding to transition states (with low barriers) between the reactants and the conical intersection seam: a mixed asynchronous/synchronous [1,2] ortho path, an asynchronous [1,3] meta path and a synchronous [1,3] meta path.

I Introduction

In general, a photochemical reaction path has two branches: a branch on the excited state and a branch on the ground state. The two branches are connected at a point where the potential energy surfaces become degenerate known as a conical intersection (CI)[1-7]. However, a conical intersection is not an isolated point, but a collection of points, which we will refer to as a conical intersection "seam"[1,8-10]. In this work we shall explore this feature in some depth for the case of the photochemical reactivity of ethylene and benzene. In the photocycloaddition of an arene and an alkene there are several possible regioselectivities (Scheme I). We will show that this regioselectivity is in part controlled by such an extended conical intersection seam.

Experimental Background: Cycloadditions with alkenes are important and characteristic photochemical reactions of aromatic compounds. The prototype example of such a photocycloaddition is the reaction of benzene with ethylene[11-22]. Three cycloaddition modes (regioselectivity) can be distinguished (See Scheme 1): ortho-cycloaddition [1,2], meta-cycloaddition [1,3], and para-cycloaddition [1,4], and many applications of these reactions in organic synthesis have been described, as they afford the possibility to obtain polycyclic compounds in one step, which is important in the design of more complex molecular frameworks.

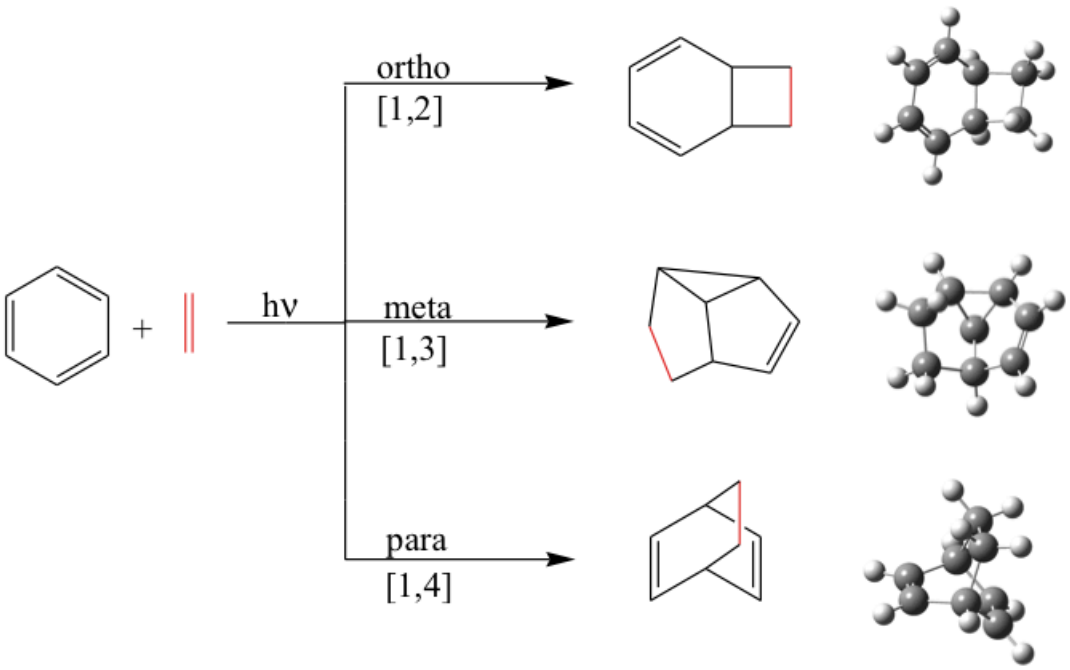

Scheme 1

The photocycloaddition reactions of arenes with alkenes have been extensively studied in order to rationalize the formation of the three possible cycloaddition products[11,16]. The meta-cycloaddition mode ([1,3] in our simplified notation) has been applied most extensively and is used as an important step in the synthesis of natural products. This is the usual outcome in the photocycloadditions of arenes + alkenes. The ortho [1,2] product is found experimentally in reactions involving arenes with electron-withdrawing substituents. Ortho addition is preferred when there is a substantial difference between the electron-donor and electron-acceptor properties of the arene and the alkene, and meta when these differences are small. Finally, the [1,4] pathway takes place in a very few cases where the steric factors are important[16] or when the alkene is an allene[23] or a diene[24,25]. In the case of the unsubstituted reactants (benzene + ethylene), the wavelength of light used in experiments[26-28] suggests that the reaction proceeds via the lowest-lying singlet excited state of benzene[11,12,15,19,21,22,26]. In this case, the ratio of meta to ortho adduct is approximately 50:50[16,29].

There are only a few theoretical discussions of this reaction. Bryce-Smith and Gilbert have described the reaction mechanism of cycloadditions using orbital symmetry rules[14,15,30]. Houk invoked frontier orbital theory to discuss the reactivity trends[17]. Mattay discussed the regioselectivities and stereoselectivities of photoreactions of arenes to olefins on the basis of an exciplex mechanism[18,31]. These selectivities were also found to be influenced by the photoinduced charge transfer and, in addition to the exciplex, dipolar intermediates were considered in order to explain the high regioselectivities of photocycloadditions with donor- and acceptor-substituted arenes. Cornelisse et al. discussed the three modes of addition using quantum chemical methods as well as qualitative molecular orbital diagrams[16,22,32,33].

Some 16 years ago we performed a CASSCF study with MMVB dynamics for S_1 benzene with ethylene [29]. These computations located an isolated conical intersection that was suggested to be important feature in the mechanism. However, the technology was not available then to study points other than minimum energy conical intersection points.

Conceptual review: In photochemistry, the first branch of the reaction pathway on the excited-state surface may be associated with a transition state (as in benzene[34]). However a transition state, in such a case, plays a slightly different role than in thermochemistry (where there is thermal equilibrium between reactants and transition state). In an excited state problem, a transition state on the excited state might be associated with a wavelength dependence (as in benzene[34]) if it lies above the “reactants” in energy. Alternatively, if it lies below the “reactants” it plays a similar role to a transition state that is “not rate determining” in a thermal reaction. Thus it may serve as a dynamical bottleneck controlling the spread of the wavepacket and directing it in a certain way. The excited state branch of the reaction co-ordinate may also contain an intermediate. The role of such intermediates will be similar to thermochemistry.

Finally, reaction paths on the ground state, after decay at the conical intersection, can be traced using dynamics[35-37] or minimum energy paths (MEPs)[38,39].

Different excited state reaction paths may encounter conical intersections at points that may or may not belong to the same conical intersection seam. In benzene. for example, there are two independent branches on the S_1/S_0 seam, which consists of at least 13 CI critical points[40]. A given point on a conical intersection seam is always associated with two diabatic electronic states, which are in turn associated with distinct VB structures or combinations of VB structures[1,41-43]. Two points on a conical intersection seam that are associated with the same pair of diabatic states are said to be on the same seam segment or branch.

For the photocycloaddition of ethylene and benzene there are 3 types of VB structure that dominate the mechanism, as shown in Scheme 2.

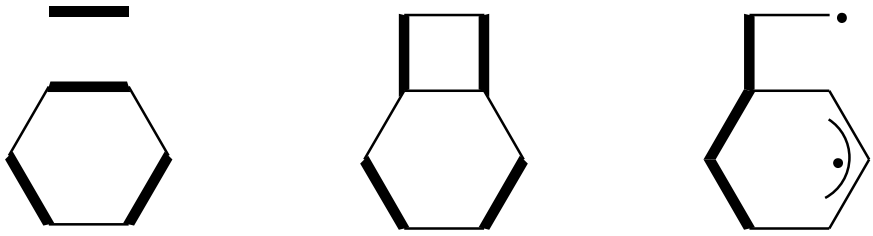

Scheme 2

In scheme 2 the light lines indicate the σ frame, while the bold lines indicate the pairing of spins. Thus the structure *R* (reactants) shows a Kekulé structure for the benzene moiety and the fully formed ethylenic π bond. The structure P_1 indicates the product-like VB structure for the ortho [1,2] case. P_2 is an open biradical. (There are similar structures for the meta [1,3] and para [1,4]).

There are also two distinct possibilities for the reaction path: synchronous, where both C-C σ bonds are formed at the same rate, or asynchronous where one bond is formed faster than the other, leading possibly to a biradical intermediate with VB structure indicated as P_2. Thus there are 3 distinct types of diabatic surfaces associated with the cycloaddition of ethylene to benzene.

The conical intersection (real crossing) seam will have two distinct segments either R/P_1 or P_2/P_1 if an intermediate is involved. In addition, one may have various transition states associated with avoided crossings of these diabatic states. Thus one would expect a transition state between reactants and a biradical minimum arising from the avoided crossing of R and P_2.

Our plan for this paper is as follows. We shall begin with a brief computational details section. Then, the discussion of the results will be divided into 2 parts. In the first part we will start with a presentation of the complex mechanism, which arises from the computations, in a rather general way. This will be followed, in the second part, with the documentation of the various reaction pathways in more detail with references to supplementary information where detailed numerical data is presented.

II Computational details

All the electronic structure computations (optimizations, MEP etc) were carried out using the CASSCF (8,8) method, with a 6-31G* basis set, in a development version [44] of Gaussian. For some points we have analyzed the effect of dynamic electron correlation on excited state energies with the CASPT2 method[7,45,46], using the program MOLCAS-7[47].

As a distinguishing feature of this work, we have also carried out a full second order analysis of critical points on the conical intersection seam. This analysis has been carried out using the methods of Sicilia et al. [8,9,48]. Using such methods we can perform frequency analysis of vibrations confined to the seam and thus we can optimize minima and transition states with the space of the seam. We can also compute minimum energy paths from a saddle point (TS) on the seam (which we shall refer to as a seam-MEP) and thus map out a segment of the seam. In addition, one can perform a 'seam-scan", performing constrained optimizations along a distinguished co-ordinate (eg torsion in a biradical), to map out a particular part of the conical intersection seam.

Reaction pathways from transition states were also characterized in forward and reverse direction by an intrinsic reaction coordinate (IRC) analysis[49,50] finding the minimum energy path (MEP).

The determination of possible reaction paths on the ground state from a CI point requires a different strategy[38,39]. There is no unique initial search vector (such as the transition vector at a transition state), so one must test several possibilities. In general we chose either i) one of the branching space vectors, ii) the gradient of one of the degenerate states, or iii) a vector connecting the CI geometry and some other structure such as a product.

In some cases the preceding strategy does not work very well. This can arise if there is a "downward direction" but no "valley". In this case we used a steepest descent path (SDP). From a given point, one follows the gradient vector (without mass-weighting) in the downhill direction with a fixed identity hessian matrix. While this path has no physical significance (unlike an MEP),

it can provide qualitative information about possible reaction paths. Thus, if the step size is sufficiently small, this procedure will terminate at the "closest" critical point. Just like an MEP from a CI, one must choose a search vector and an initial geometry along this direction. At a conical intersection there are two gradients (one for each surface) and one must follow both gradients for a peaked conical intersection[51]. For a sloped conical intersection both gradients are almost the same. Thus in practice, at a conical intersection point the geometry was distorted in both directions along the gradient difference vector scaled by a factor of 0.1. Of course, in cases where both MEP and SDP were possible, the end point was the same.

The SDP procedure, just described, can also be used at a TS or a point with two imaginary frequencies (a second order saddle point, labeled sp2 here). In such cases, the geometry was distorted in the direction of the imaginary frequency (frequencies), in both directions, in order to have a non-zero gradient vector to follow. In other words, at a second order saddle point (2 imaginary frequencies), one must begin with a small step associate with each normal co-ordinate.

We also wish to understand the electronic origin of the conical intersection seam in terms of the VB structures shown in scheme 2. To obtain this information, we have performed a VB analysis of the ground and excited state wavefunctions at points on the conical intersection seam. This analysis was carried out by computing the VB wavefunctions using the MMVB method[52] and, in some cases, performing an analysis of spin exchange density matrix[53] obtained with CASSCF. The numerical results were similar.

Finally because there are many structures to discuss, and because we can have transition states both in the normal way and (saddle points) on the conical intersection seam we need a specialized notation to distinguish between such structures. We have adopted the following general notation:

$$(syn/asyn)^{[1,2]/[1,3]/[1,4]/[1,X]}_{\min/TS/sp2/scan} S_1/S_0/CI\{\text{point group}\}$$

to distinguish
i) the synchronicity (*syn / asyn*),
ii) the regioselectivity (superscript: [1,2]…),
iii) the nature of the structure (subscript: minimum min; transition state *TS*; second order saddle point *sp2*; partial optimization *scan*),
iv) the adiabatic state (denoted S_1 or S_0) or an S_1/S_0 conical intersection (denoted CI), and
v) {point group symmetry}.

Thus, for example, $(asyn)^{[1,3]}_{\min} CI\{C_1\}$ refers to an asynchronous minimum on the conical intersection seam for [1,3] regioselectivity with C_1 point group symmetry, while $(asyn)^{[1,3]}_{TS} S_1\{C_1\}$ refers to a transition state on the S_1 surface with C_1 symmetry. Notice that we use TS for a "real" transition structure on an adiabatic surface and for a saddle point on the conical intersection seam.

III Results and discussion

Irrespective of the regioselectivity, there are 3 main steps associated with the photochemical path from reactants to products. The first step involves the reaction path from the reactants to the conical intersection seam, possibly involving a transition state and/or intermediates. The second step involves radiationless decay at the conical intersection seam itself. Finally, the third step involves ground state reaction paths that become possible via the decay at the conical intersection. As mentioned in the introduction, the conical intersection seam is the central feature of any mechanistic discussion. A wavepacket must cross the extended conical seam which divides the two branches of the reaction path. The shape and extent of this seam determines the range of geometries that can proceed to the third phase involving pathways on the ground state. Of course, as discussed in the introduction, there may be transition states and intermediates on S_1 that also control the shape of the wavepacket that ultimately reaches the seam.

We shall present our results by firstly giving a "map" in Figures 1-3 of the structures studied in computations. Then we shall discuss the 3 steps of the reaction mechanism (in three subsections) from a general mechanistic point of view. Following this we shall present the documentation (again in three subsections) that supports the mechanistic discussion.

Overview of the computational results: In Figures 1 and 2 we have illustrated the mechanistic pathways that have been studied computationally in this work. In Figure 3 we show the energetics and connectivity of the conical intersection seam. Each figure contains the labels of the structures that have been optimized (eg. Fig 1, where $(syn)^{[1,2]}_{\min} CI\{C_1\}$ indicates a minimum energy point on the conical intersection seam with 1,2 regioselectivity). Associated with each structure is the energy (kcal mol^{-1}) relative to S_1 benzene + ethylene. Thus positive energies lie above S_1 benzene + ethylene (computed as a supermolecule in the same basis). Minimum energy paths are illustrated with solid lines with arrows (eg. Fig 1, where there is an MEP from the TS $(asyn)^{[1,2]}_{TS} S_1\{C_1\}$ to the seam point $(syn)^{[1,2]}_{\min} CI\{C_1\}$). Finally, we show steepest decent paths (SDP, see computational details for a definition) as dotted lines with arrows (eg Fig 1, the second order saddle point $(syn)^{[1,2]}_{sp2} S_1\{C_s\}$ is connected to $(syn)^{[1,2]}_{TS} S_1\{C_s\}$ along one direction of negative curvature and to $(asyn)^{[1,X]}_{\min} S_1\{C_s\}$ along the other).

From Fig 1 and Fig 2 it can be seen that there are two overlapping "active" mechanistic pathways corresponding to transition states between the reactants and the conical intersection seam. These have been indicted with bold lines in color in Figures 1 and 2. This topology yields three reaction

paths: i) red line in Figures 1 and 2 corresponding toa mixed asynchronous/synchronous [1,2] path: $(asyn)_{TS}^{[1,X]}S_1\{C_s\}$, $(asyn)_{\min}^{[1,X]}S_1\{C_s\}$, $(asyn)_{TS}^{[1,2]}S_1\{C_1\}$ to $(syn)_{\min}^{[1,2]}CI\{C_1\}$ ii) blue line in Figure 2 corresponding to the asynchronous [1,3] path $(asyn)_{TS}^{[1,X]}S_1\{C_s\}$, $(asyn)_{\min}^{[1,X]}S_1\{C_s\}$, $(asyn)_{TS}^{[1,3]}S_1\{C_1\}$ and finally $(\text{asyn})_{\min}^{[1,3]}CI\{C_1\}$ and 3) green line in Figure 2, corresponding to a synchronous [1,3] path: $(syn)_{TS}^{[1,3]}S_1\{C_s\}$ to $(syn)_{TS}^{[1,3]}CI\{C_s\}$ The synchronous 2_s+2_s, [1,2] pathway is shown in Figure 1 (center) together with the two (equivalent) related asynchronous biradical paths (top/bottom). The asynchronous path way is shown twice (top/bottom) to emphasize the relationship between two corresponding related asynchronous paths and the $(asyn)_{TS}^{[1,2]}S_1\{C_1\}$ transition state connects them and the corresponding conical intersections. The two possible [1,3] pathways are shown in Figure 2: 1) the synchronous [1,3] meta approach (green bottom, Figure 2), and 2) an asynchronous [1,3] biradical intermediate pathway (center, blue). The asynchronous [1,2] path shares the biradical intermediate $(asyn)_{\min}^{[1,X]}S_1\{C_s\}$ with the [1,3] path.

In Figure 1 and 2, the structures we have optimized on the conical intersection are connected by dashed lines. The connectivity and relative energetics of the conical intersection points is illustrated in Figure 3. Notice that there are two conical intersection seams; one for synchronous (SYN in Figure 3) and one for asynchronous (ASYN); howver, they can be connected either by a “seam-MEP” or a “seam-SCAN” as shown in Figure 3.

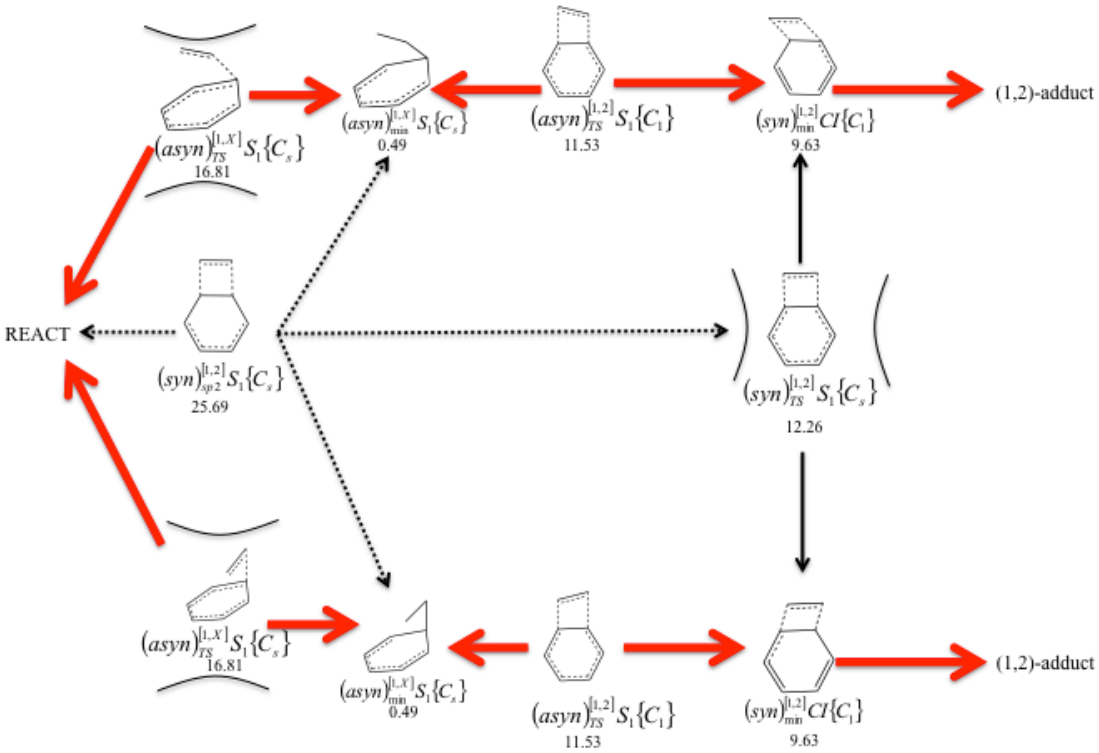

Figure 1. Schematic map of the important critical points associated with the 1,2 regioselectivity of ethylene + benzene on S_1. Energies relative to the S_1 state of benzene + ethylene (S_0) in kcal mol^{-1}. Solid arrows indicate MEP dashed arrows indicate SDP (See also sections F-I in supporting information as well as Table S-V for further details (animations, tables and graphs of interpolations, MEP and SDP). The highlighted red arrows indicate the mixed asynchronous/synchronous [1,2] path: $(asyn)_{TS}^{[1,X]} S_1\{C_s\}$, $(asyn)_{\min}^{[1,X]} S_1\{C_s\}$, $(asyn)_{TS}^{[1,2]} S_1\{C_1\}$ to $(syn)_{\min}^{[1,2]} CI\{C_1\}$

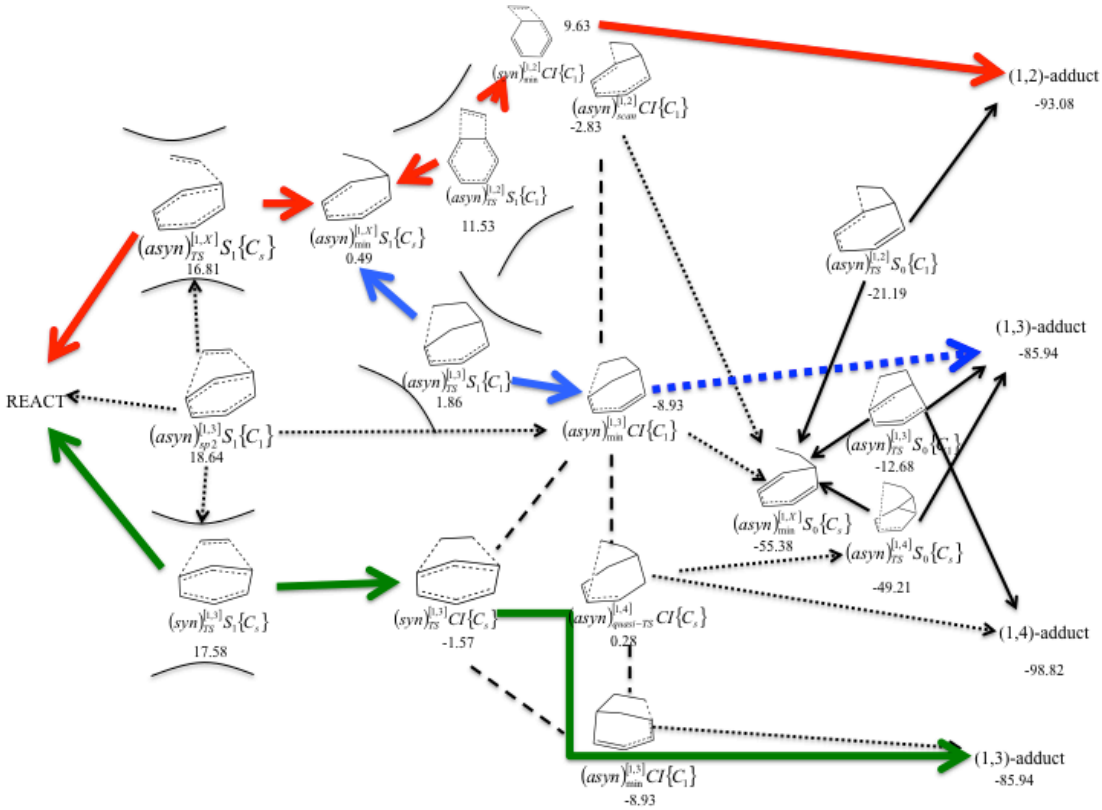

Figure 2. schematic map of the important critical points associated with the (1,2)-(1,3) regioselectivity. The topology of the surface around the various TS is indicated wit the pairs of concave lines. Energies are S_1 state of benzene + ethylene (S_0) in kcal mol^{-1} (See also sections F-I in supporting information as well as Table S-V for further details (animations, tables and graphs of interpolations, MEP and SDP). Dashed lines mean paths within the seam.

The highlighted paths (colored) correspond to: red, the mixed asynchronous/synchronous [1,2] path: $(asyn)_{TS}^{[1,X]} S_1\{C_s\}$, $(asyn)_{\min}^{[1,X]} S_1\{C_s\}$, $(asyn)_{TS}^{[1,2]} S_1\{C_1\}$ to $(syn)_{\min}^{[1,2]} CI\{C_1\}$ Blue: the asynchronous [1,3] path $(asyn)_{TS}^{[1,X]} S_1\{C_s\}$, $(asyn)_{\min}^{[1,X]} S_1\{C_s\}$, $(asyn)_{TS}^{[1,3]} S_1\{C_1\}$ and finally $(\text{asyn})_{\min}^{[1,3]} CI\{C_1\}$ green: synchronous [1,3] path: $(syn)_{TS}^{[1,3]} S_1\{C_s\}$ to $(syn)_{TS}^{[1,3]} CI\{C_s\}$

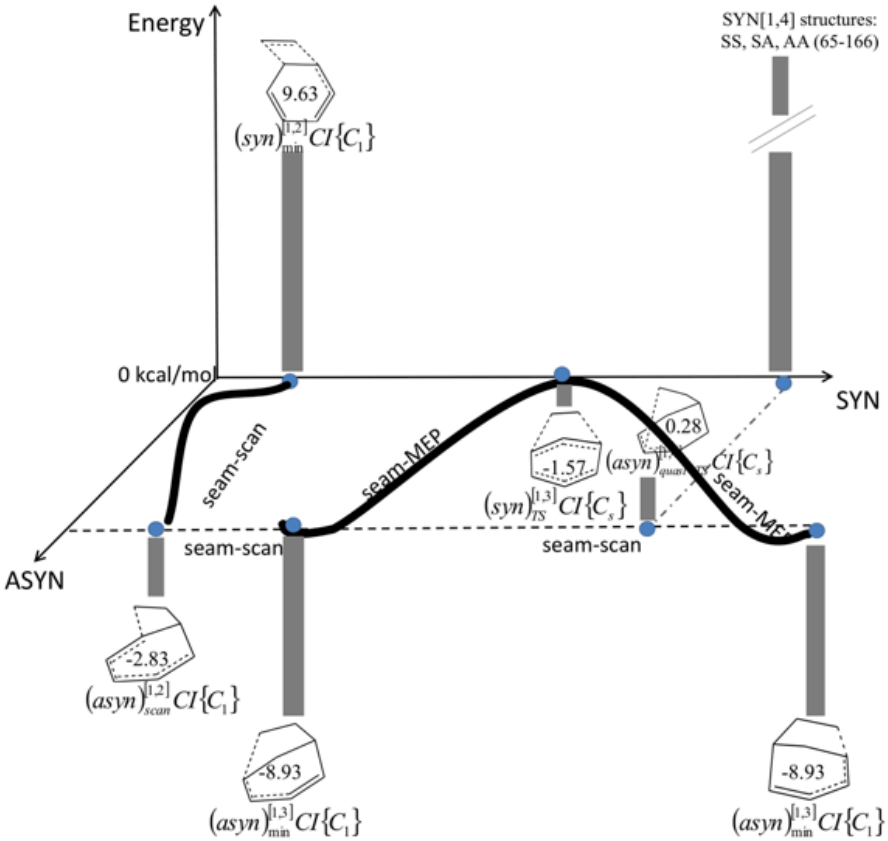

Figure 3: Energies and connectivity of points on the conical intersection seam for the asynchronous (ASYN y axis) and the synchronous (SYN x axis) approach. The connectivity (solid heavy lines) is either by a seam-MEP (ie reaction path constrained to lie within the seam) or a seam-scan (where the torsional co-ordinate is selected as a distinguished variable and the CI point is optimized under constraint) Energies relative to S_1 state of benzene + ethylene (S_0) in kcal mol^{-1}. For the seam-scan between $(asyn)^{[1,2]}_{scan} CI\{C_1\}$ and $(syn)^{[1,2]}_{min} CI\{C_1\}$, see Fig. S-19; for the seam-scan $(asyn)^{[1,4]}_{quasi-TS} CI\{C_s\}$ $(asyn)^{[1,3]}_{min} CI\{C_1\}$ $(asyn)^{[1,2]}_{scan} CI\{C_1\}$, see Fig. S-3; and for the seam-MEP see Figs. S-2 and S-20.

The extended conical intersection seam: Our discussion will now be focused on the conceptual aspects of the conical intersection seam, as shown in Figures 3, 4 and 5. We begin with a discussion of the asynchronous conical intersection seam. In Figure 4 we show (schematically) the extended conical intersection seam associated with the asynchronous pathways comprising the optimized critical points $(asyn)^{[1,2]}_{scan} CI\{C_1\}$, $(asyn)^{[1,3]}_{min} CI\{C_1\}$ and $(asyn)^{[1,4]}_{quasi-TS} CI\{C_s\}$ (corresponding to the ASYN co-ordinate in Figure 3). The additional point $(asyn)^{[1,2]}_{scan} CI\{C_1\}$ (we could not find a critical point in this region) was obtained by a torsional coordinate constrained conical intersection optimization[48] (ie seam-scan). The diabatic surfaces associated

with the asynchronous seam (Figure 4) are labeled P_1 and P_2 (see Scheme 2) and this aspect will be discussed later. The maximum on the seam $(asyn)^{[1,4]}_{quasi-TS} CI\{C_s\}$ is only a very shallow local minimum (hence the notation *quasi-TS*). An [1,4] asynchronous S_1 path passes along a ridge on S_1, (which can also be seen in Figure 4), separating the two symmetry equivalent versions of $(asyn)^{[1,3]}_{\min} CI\{C_1\}$.

It is clear from Figure 3 and Figure 4 that $(asyn)^{[1,3]}_{\min} CI\{C_1\}$ is the lowest energy point on the seam. However, $(asyn)^{[1,2]}_{scan} CI\{C_1\}$ has only a slightly higher energy (see Figure 3). But it is also clear that $(asyn)^{[1,4]}_{quasi-TS} CI\{C_s\}$ is significantly higher in energy. Furthermore $(asyn)^{[1,4]}_{quasi-TS} CI\{C_s\}$ is effectively a saddle point on the seam. It is not immediately obvious how one can interpret this mechanistically. (ie although $(asyn)^{[1,4]}_{quasi-TS} CI\{C_s\}$ is seam saddle point, there can, of course, never be a reaction path that remains on the seam following the seam mode associated with the imaginary frequency). However, one can still expect radiationless decay to occur near minima on the seam rather than maxima. Further, as one can see in Figure 4, the asynchronous [1,4] structures are associated with a "ridge" in the P_1 energy sheet and the seam itself. Thus the lowest energy parts of the asynchronous part of the seam are associated with [1,3] or [1,2] regioselectivity.

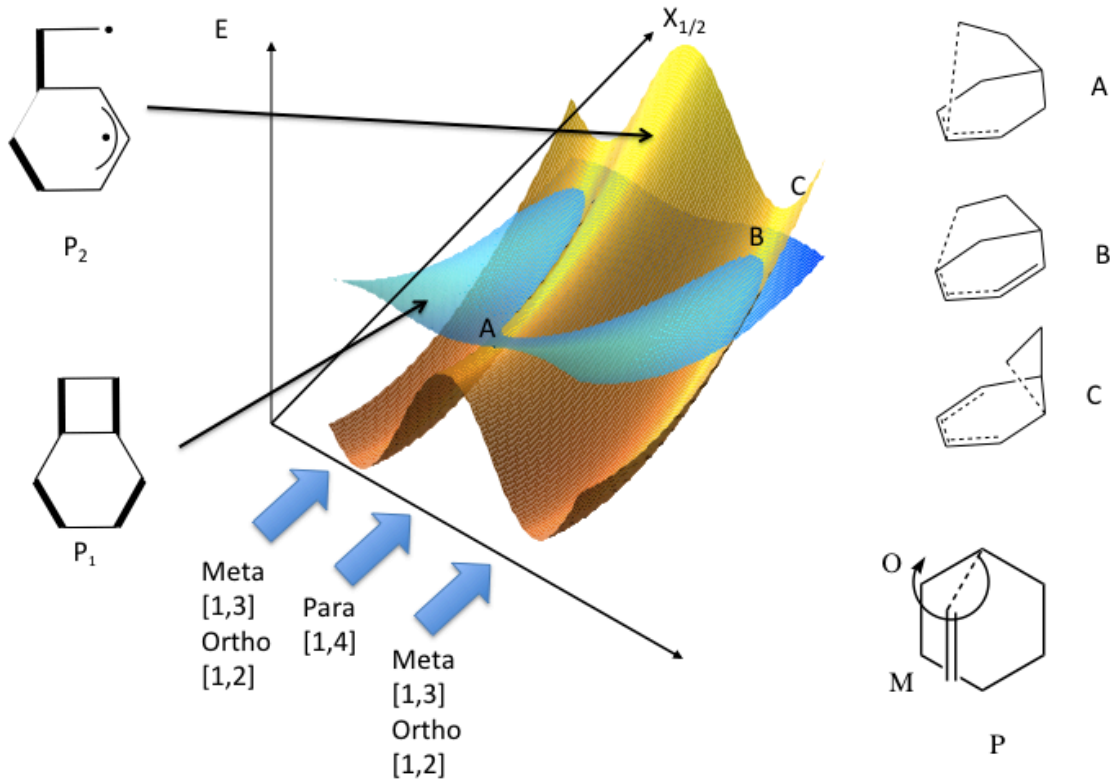

Figure 4. Conical Intersection seam associated with the asynchronous reaction pathways. The diabatic states are P, and P_2 (see Scheme 2). In the "label" of the x axis we indicate the torsional angle in the seam-scan, and the points O (1,2) Ortho, M (1,3) Meta and P (1,4) Para

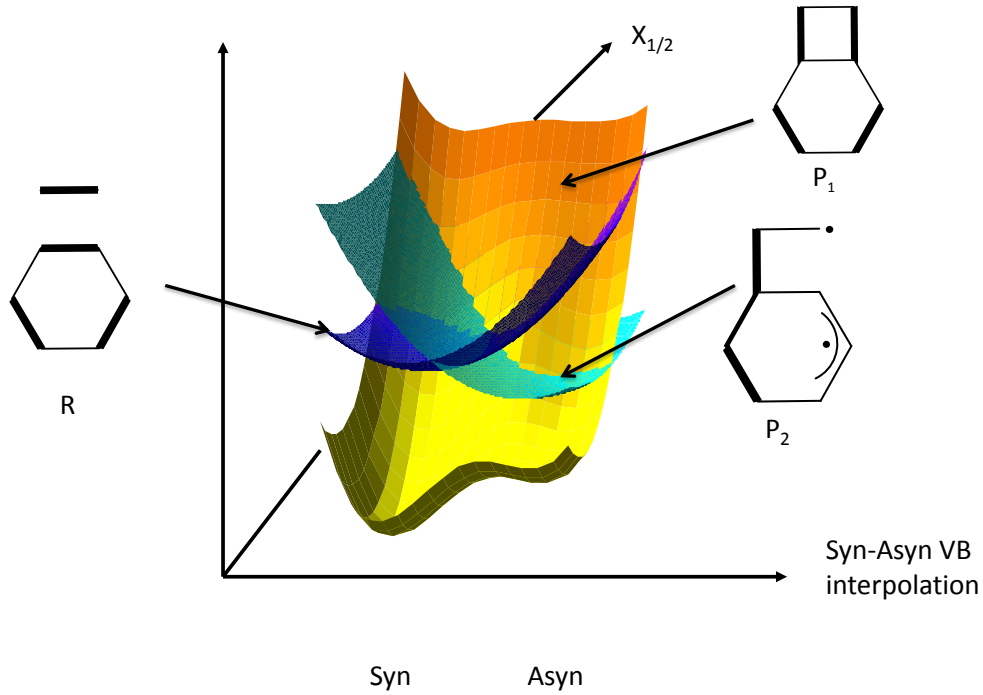

Figure 5. Interpolation between $(asyn)^{[1,2]}_{scan} CI\{C_1\}$ and $(syn)^{[1,2]}_{\min} CI\{C_1\}$ conical intersections.

Here we have 3 VB diabatic states (R, P_1 and P_2) seam-scan in Figure 3.

We now discuss the conical intersection seam associated with the synchronous pathways (axis labeled SYN in Figure 3). In Figure 5 we show a schematic representation of this conical intersection along the co-ordinate, labeled seam-scan, connecting $(asyn)^{[1,2]}_{scan} CI\{C_1\}$ and $(syn)^{[1,2]}_{\min} CI\{C_1\}$ in Figure 3 and shown as Syn-Asyn VB interpolation in Figure 5. (A similar topography is present along the co-ordinate from $(syn)^{[1,3]}_{TS} CI\{C_s\}$ to $(asyn)^{[1,3]}_{\min} CI\{C_1\}$ in Figure 3, except the R and P_2 surfaces cross at the maximum $(syn)^{[1,3]}_{TS} CI\{C_s\}$). The origin of the saddle point (TS) on the seam is the avoided crossing shown in Figure 5 that we shall discuss subsequently. From Fig 3 it is clear that $(syn)^{[1,2]}_{\min} CI\{C_1\}$ is much higher in energy than the asynchronous seam points. Further, while $(syn)^{[1,3]}_{TS} CI\{C_s\}$ has a lower energy, it is a saddle point on the seam; and it can be interpreted in the same way as $(asyn)^{[1,4]}_{quasi-TS} CI\{C_s\}$. Notice that there is a second order saddle point on S_1 $(asyn)^{[1,3]}_{sp2} S_1\{C_1\}$ where one imaginary frequency connects $(syn)^{[1,3]}_{TS} S_1\{C_s\}$ and $(asyn)^{[1,X]}_{TS} S_1\{C_s\}$ and the other connects $(asyn)^{[1,3]}_{\min} CI\{C_1\}$ and the reactants.

To summarize, using Figure 3. If we ignore, for the moment, any structures on S_1 for the moment, then the shape and energetics of the asynchronous conical intersection seam, suggests that 1,2 and 1,3 will be the preferred regioselectivities with similar weight. The syn 1,3 seam (CI) structure is a local maximum on the seam. Further, the synchronous 1,2 structure lies much higher in energy. The syn 1,4 regioselectivity seems impossible on the basis of energetics and the asynchronous 1,4 path is associated with a maximum on the seam.

We now discuss the origin of the shape on the conical intersection seam in using VB arguments and Figure 4 and 5. In general, a transition structure (ie saddle point) on the seam can arise i) through steric repulsion on the seam (viz. $(asyn)^{[1,4]}_{\text{quasi-TS}} CI\{C_s\}$ in Figure 4 or ii) because of an avoided crossing between two states (Figure 5) which form one of the "partners" of the degenerate pair of states (in the limit this would be a 3-fold intersection[54-56]). In Figure 5 we show the second case above. The synchronous and asynchronous segments of the conical intersection seam can be connected (using an interpolation between $(asyn)^{[1,2]}_{scan} CI\{C_1\}$ and $(syn)^{[1,2]}_{\min} CI\{C_1\}$ as an example). The crossing seam begins (left Figure 5) as R/P_1 at $(syn)^{[1,2]}_{\min} CI\{C_1\}$ and ends (right Figure 5) as P_1/P_2 at $(asyn)^{[1,2]}_{scan} CI\{C_1\}$. Thus there is a continuous crossing seam between $(syn)^{[1,2]}_{\min} CI\{C_1\}$ and $(asyn)^{[1,2]}_{scan} CI\{C_1\}$ with an avoided crossing (actually shown as a real crossing in Figure 5) between one of the two degenerate partner diabatic states R and P_2. (A similar feature

connects $(syn)_{TS}^{[1,3]}CI\{C_s\}$ and $(asyn)_{\min}^{[1,3]}CI\{C_1\}$). Thus the synchronous and asynchronous segments of the conical intersection seam are connected via the topology shown in Figure 5. In contrast, the various asynchronous points on the conical intersection are connected via the type of surface shown in Figure 4. Here the maximum on the surface is determined mainly by steric considerations. The preceding discussion can be useful in predicting and understanding substituent effects. Thus bulky substituents may change the shape of the asynchronous seam (Figure 4). While substituents that stabilize different radical centers may affect the relative behavior of P_1 and P_2.

Reaction paths on S_1 We now discuss salient features of the three S_1 paths: i) (red in Figures 1 and 2) a mixed asynchronous/synchronous [1,2] path: $(asyn)_{TS}^{[1,X]}S_1\{C_s\}$, $(asyn)_{\min}^{[1,X]}S_1\{C_s\}$, $(asyn)_{TS}^{[1,2]}S_1\{C_1\}$ to $(syn)_{\min}^{[1,2]}CI\{C_1\}$ ii) (blue in Figure 2) the asynchronous [1,3] path $(asyn)_{TS}^{[1,X]}S_1\{C_s\}$, $(asyn)_{\min}^{[1,X]}S_1\{C_s\}$, $(asyn)_{TS}^{[1,3]}S_1\{C_1\}$ and finally $(\mathrm{asyn})_{\min}^{[1,3]}CI\{C_1\}$ and 3) (green in Figure 2) a synchronous [1,3] path: $(syn)_{TS}^{[1,3]}S_1\{C_s\}$ to $(syn)_{TS}^{[1,3]}CI\{C_s\}$.

There are two important transition states $(asyn)_{TS}^{[1,X]}S_1\{C_s\}$ and $(syn)_{TS}^{[1,3]}S_1\{C_s\}$ which form the dynamical bottleneck on the path to the conical intersection seam. These two structures, which form the barrier between the reactants and the CI seam or the intermediate, are very close in energy. We have also carried out CASPT2 computations (see supporting information) on these three structures. In both cases, the activation energy becomes negative (ie the energy is below S_1 benzene + ethylene). This clearly indicates the need to re-optimize the geometries at the CASPT2 level (which is not feasible technically). But it also suggests that the barrier heights might be quite small and this could be consistent with the fact that no wavelength dependence is observed experimentally [11]. Thus the important point is that these transition states serve mainly to restrict the spread of the wavepacket (dynamical bottleneck) directing it towards the seam. (ie transition state theory that assumes thermal equilibrium between the TS and reactants is not applicable)

We now begin a discussion of the main features of the S_1 [1,2] reaction pathway. As one can see from Figure 1, the potential energy surface for the synchronous [1,2] pathway is very similar to that for classic ethylene + ethylene[57] and other 2+2 cycloadditions[58]. There are two CI points equivalent by symmetry denoted $(syn)_{\min}^{[1,2]}CI\{C_1\}$ interconnected by a transition state on S_1, $(syn)_{TS}^{[1,2]}S_1\{C_s\}$. Each CI point has almost equal C-C partly formed σ bonds (hence the notation syn). However, there is no "real" synchronous [1,2] pathway from reactants: instead of a transition state along a C_s reaction path, one finds a point with two imaginary frequencies (a local mountain top), denoted $(syn)_{sp2}^{[1,2]}S_1\{C_s\}$. The extra negative direction of curvature leads to the two equivalent lower energy asynchronous biradical pathways, shown in red in Figure1, passing via a biradical intermediate $(asyn)_{TS}^{[1,X]}S_1\{C_s\}$.

Now we turn to the synchronous [1,3] pathway (green in Figure 2) and the asynchronous biradical pathways (blue in Figure 2). These two pathways have the initial transition states $(syn)_{TS}^{[1,3]} S_1\{C_s\}$ (Figure 2, bottom) and $(asyn)_{TS}^{[1,X]} S_1\{C_s\}$ (Figure 2, top) (where we use the superscript [1,*x*] to indicate an open biradical structure with no secondary C-C σ bond). These pathways are separated by a second-order saddle point (i.e. mountain top), denoted as $(asyn)_{sp2}^{[1,3]} S_1\{C_1\}$.

From the biradical intermediate $(asyn)_{\min}^{[1,X]} S_1\{C_s\}$., there are 2 active reaction paths to the seam via S_1 transition states: 1) (red in Figure 2) via $(asyn)_{TS}^{[1,2]} S_1\{C_1\}$ leading to $(syn)_{\min}^{[1,2]} CI\{C_1\}$, that we have just discussed and 2) via (blue in Figure 2) $(asyn)_{TS}^{[1,3]} S_1\{C_1\}$ leading to $(asyn)_{\min}^{[1,3]} CI\{C_1\}$. A [1,4] path is also possible. However, we were unable to optimize a true transition state. Beginning at the maximum of a linear interpolation between $(asyn)_{\min}^{[1,X]} S_1\{C_s\}$ and $(asyn)_{quasi-TS}^{[1,4]} CI\{C_s\}$ (a minimum with a very small positive frequency), we found only an "orthogonal" TS connecting two equivalent [1,3] pathways. (See section E in supporting information for further details.) Thus the 1,4 path appears to be located on a ridge between asynchronous 1,3 approaches (see Figure 4, also the 1,4 is also a "ridge" on the conical intersection seam).

There remains the question about whether there is a possible [1,2] path via the biradical intermediate $(asyn)_{\min}^{[1,X]} S_1\{C_s\}$ that does not pass via $(asyn)_{TS}^{[1,2]} S_1\{C_1\}$ and but rather leads to the asynchronous part of the conical intersection seam. A linear interpolation between $(asyn)_{\min}^{[1,X]} S_1\{C_s\}$ and a point $(asyn)_{scan}^{[1,2]} CI\{C_1\}$ on the seam passed through a maximum at 14.01 kcal mol^{-1}. However, we were not able to find a true transition state. Thus it is most likely that the [1,2] transition structure lies on the "side" of the [1,3] asynchronous valley as shown in structure C in Figure 4. (see section E in supporting information)

Reaction pathways on S_0 It now remains to briefly discuss the final phase of the reaction paths; namely, from the conical intersection seam to products on S_0. To document such paths one might use dynamics. Here we have chosen (for many examples) to simply follow a path of steepest decent (SDP), following the gradient vector with small step sizes (see computational details). In some cases the ground state reaction path is clear. For example, we can see that $(syn)_{TS}^{[1,3]} CI\{C_s\}$ (Figure 2) has an SDP that terminates directly at a [1,3] adduct and an SDP that goes back to the ground state reactants (characteristic of a "peaked" conical intersection). The situation for the asynchronous pathways from the conical intersection is less clear. On the one hand, we can find an SDP from $(asyn)_{\min}^{[1,3]} CI\{C_1\}$ to a 1,3 adduct. On the other

hand, there is a backward SDP that terminates at a ground state biradical minimum $(asyn)^{[1,X]}_{\min} S_0\{C_s\}$. There may be low energy reaction paths to products from this minimum both towards products and towards reactant. However, this aspect has not been investigated in this work. It is clear that one would need dynamics computations to determine the ratios of products that have their origin at $(asyn)^{[1,X]}_{\min} S_0\{C_s\}$. However, one would expect the "forward" path to dominate because of the momentum developed at the transition state bottlenecks in the S_1 asynchronous biradical region.

Summary of computational results for the conical intersection seam. Our purpose in this subsection (and in the two subsequent subsections), is to provide only main computational results that "document" the conceptual discussion that we have just given. We begin with the conical intersection seam. Here we have 3 elements of the computational work that need documentation: 1)the characterization of the branching space of the conical intersection, 2)characterization of any negative curvature on the seam (imaginary frequencies) and 3)VB analysis of the seam.

The relative energies of the seam points are collected in table II along with the C-C distances. The Cartesian coordinates, branching space vectors etc. are to be found in supporting information (table S-II). We were not able to find a critical point for the asynchronous [1,2] path on the seam. We did a torsional co-ordinate driven scan[48]. The corresponding energy profile is in supporting info (see Figure S-3). The structure $(\mathrm{asyn})^{[1,2]}_{scan} CI\{\mathrm{C}_1\}$ in Table II is from this scan.

Table I. Characterization of the S_1/S_0 seam. See section A in supporting information for additional data (geometries and vectors) as well as Table S-II (animation of branching space vectors and imaginary frequencies).

Point	ΔE^a (kcal/mol)	Distance[b] (Å)
$(syn)^{[1,2]}_{\min} CI\{C_1\}$	9.63	2.08/2.11
$(asyn)^{[1,2]}_{scan} CI\{C_1\}$	-2.83	1.59/2.52 (ortho); 2.43 (meta)[c]
$(syn)^{[1,3]}_{TS} CI\{C_s\}$	-1.57	2.02/2.02
$(asyn)^{[1,3]}_{\min} CI\{C_1\}$	-8.92	1.59/2.31
$(asyn)^{[1,4]}_{quasi-TS} CI\{C_s\}$ [d]	0.28	1.58/3.25

[a] Relative to the S_1 energy of benzene + ethylene at S_0 geometries and at a distance of 10 Å. [b] Distance between the two pairs of reactive carbon atoms in ethylene and benzene. [c] It may be considered an "ortho" structure, but actually is half in between ortho and meta. [d] It is a minimum, but the lowest positive frequency is very small.

We shall illustrate the characterization of a point on the conical intersection seam with two examples, the reader is referred to supporting information for further examples. We begin with $(syn)^{[1,3]}_{TS} CI\{C_s\}$. The branching space at a

conical intersection is spanned by the two vectors that lift the degeneracy at the apex of the cone. These are shown for $(syn)_{TS}^{[1,3]}CI\{C_s\}$ in Figure 6. It can be seen one of these the vectors, the gradient difference in Fig. 6a, is the same as the reaction co-ordinate. The other vector (gradient of the interstate coupling vector) is a skeletal deformation. So the passage through this point is like “sand in a funnel” along the reaction co-ordinate (ie the reaction path leads, in the branching space, directly to the crossing [1]).

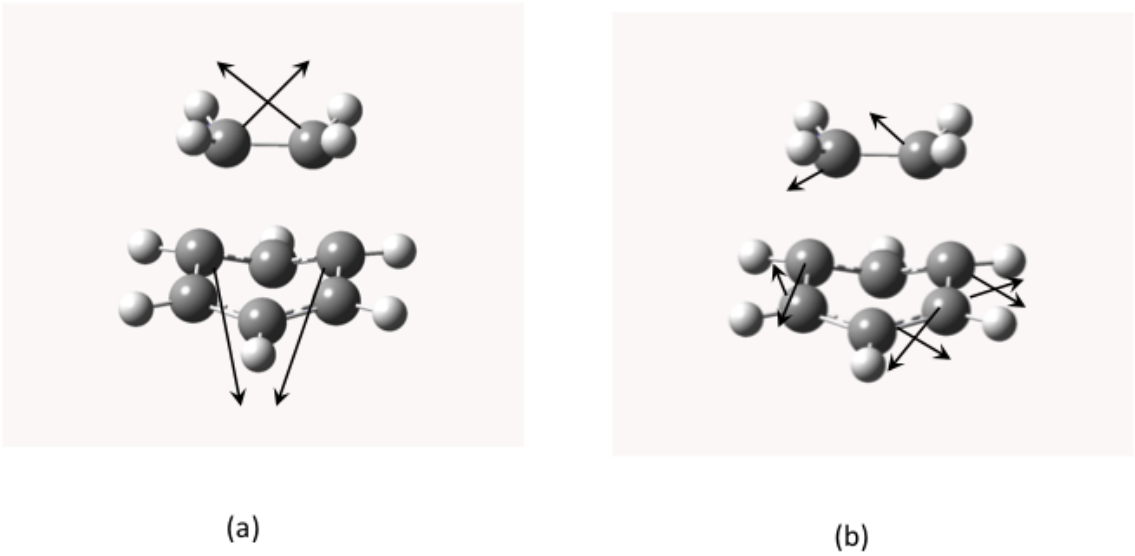

Figure 6 Branching space for a) Gradient difference b) Gradient of the interstate coupling vector (See supporting information for Cartesian co-ordinates and animations)

The idea of a transition state on the conical intersection seam has already been discussed. If one looks at the seam shown in Figure 5 it clearly passes through a maximum. The difference with respect to a conventional TS lies in the direction of the vector corresponding to the imaginary frequency, which lies entirely in the curvilinear coordinate space of the seam (which is the “join” in Figure 4). We now give a simple example. In Figure 7 we show a sketch of the transition vector for $(syn)_{TS}^{[1,3]}CI\{C_s\}$. It connects two equivalent $(asyn)_{\min}^{[1,3]}CI\{C_1\}$ points on the seam. The seam MEP from this transition state is given in supporting information (See Tables S-V, S-XXV and Fig. S-20)

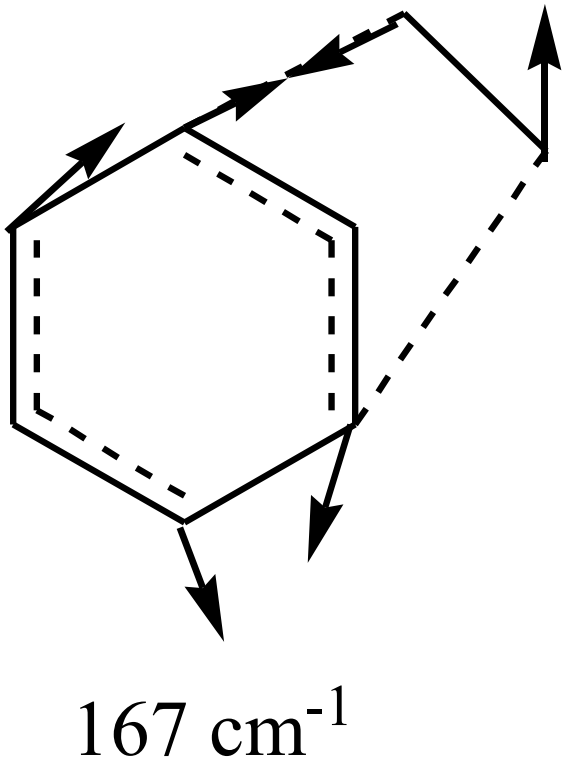

Figure 7. Transition vector for $(syn)_{TS}^{[1,3]}CI\{C_s\}$. See also Figure S-2 in supporting information.

As a second example, we mention briefly the branching space (Figure 8) for a high symmetry point, $(asyn)_{\text{quasi-TS}}^{[1,4]}CI\{C_s\}$, on the asynchronous part of the seam. Notice the large component of the reaction path in the gradient difference coordinate, corresponding to a “sand in the funnel” passage through the conical intersection.

The branching space for the remaining conical intersection points can be found in supporting information (See section A and Fig. S-4 in supporting information) The corresponding analysis of other points on the seam is collected in supporting information.

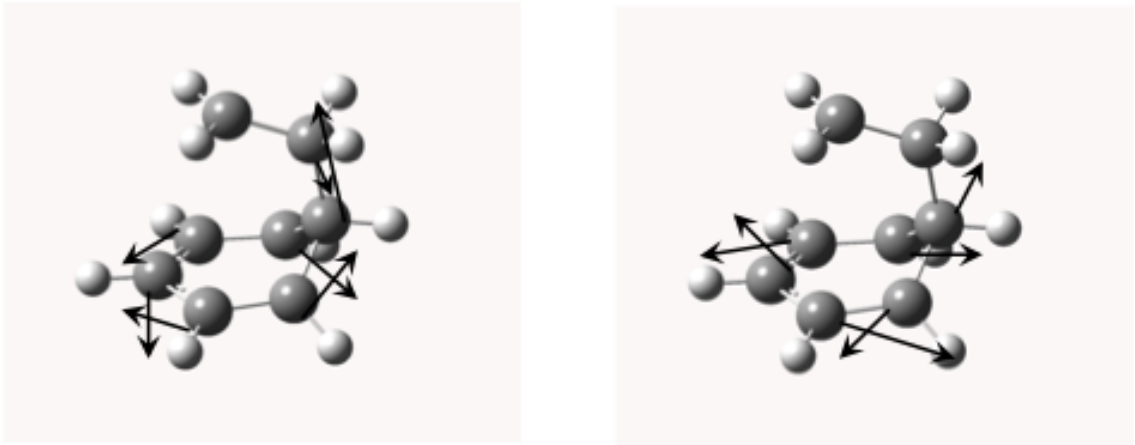

(a) (b)

Figure 8 Branching space for $(asyn)^{[1,4]}_{\text{quasi-TS}}\, CI\{C_s\}$ a) Gradient difference b) Gradient of the interstate coupling vector (See supporting information for Cartesian co-ordinates and animations)

We now turn our attention to computed VB results that support the picture of the conical intersection seam presented in Figures 4 and 5. Our objective is to show that the VB labels R, P_1 and P_2 can be obtained from computational results.

Simple VB models can be used to rationalize conical intersections[1,41,42,59]. In VB theory, spin coupled electron pairing (like the Heitler-London treatment of H_2) corresponds to chemical bonds. To extract a VB picture we have computed the spin-exchange density matrix elements[52,53] using the MMVB model[52]. The results are collected in numerical form in supporting info (See Tables S-VI to S-IX) and illustrated pictorially in Figure 9. In Figure 9 we show, as solid lines, the dominant spin couplings obtained from the numerical spin-exchange density matrix elements[52,53]

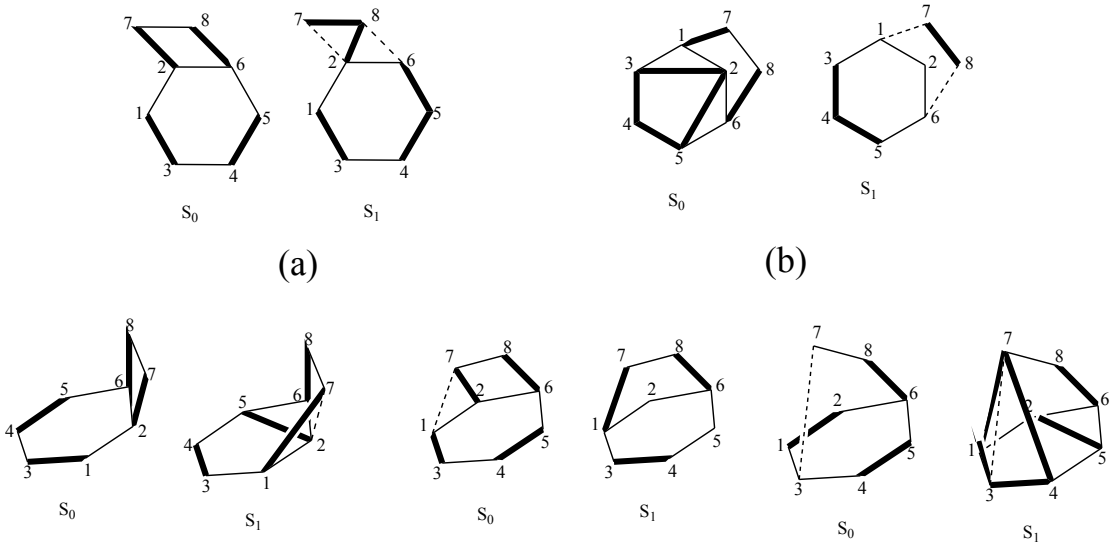

Figure 9 Computed VB analysis of (a) ,(b) $(syn)_{TS}^{[1,3]}CI\{C_s\}$, (c) $(asyn)_{scan}^{[1,2]}CI\{C_1\}$, (d) and (e) $(asyn)_{quasi-TS}^{[1,4]}CI\{C_s\}$.Tables S-VI and S-VII in supporting information contain the numerical data

The important interactions to be considered are: 1) the 8-7 linkage, corresponding to the ethylenic C-C π bond, 2) the 8-6 linkage, corresponding to one of the forming C-C σ bonds, 3) three remaining possible incipient C-C σ bonds, corresponding to the linkage 7-2 (ortho [1,2]), the linkage 7-1 (meta [1,3]), and the linkage 7-3 ([1,4] (para). The assignment of these structures as P_1, P_2 or R according to Scheme 2 and Figures 3 and 4 is given in Table III. We now give the analysis for $(syn)_{\min}^{[1,2]}CI\{C_1\}$ as an example. For S_0 we have spin couplings 7-2 and 8-6 corresponding to 2 incipient C-C σ bonds; while for S_0 we have the ethylenic C-C π bond coupling 8-7, indicative of the R VB isomer. The assignments in Table III are thus consistent with the labels in Figs. 3 and 4, confirming the qualitative VB analysis of the seam in the mechanistic section.

Table III Assignment of VB structures in Figure 8.

Structure	S_0	S_1
$(syn)_{\min}^{[1,2]}CI\{C_1\}$	**P_1**	**R**
$(syn)_{TS}^{[1,3]}CI\{C_s\}$	**P_1**	**R**
$(asyn)_{scan}^{[1,2]}CI\{C_1\}$	**P_1**	**P_2**
$(asyn)_{\min}^{[1,3]}CI\{C_1\}$	**P_1**	**P_2**
$(asyn)_{quasi-TS}^{[1,4]}CI\{C_s\}$	**P_2**	**P_1**

We have also carried out a VB analysis along the MEP from $(syn)_{TS}^{[1,3]}CI\{C_s\}$ to $(asyn)_{\min}^{[1,3]}CI\{C_1\}$ (supporting information Tables S-VIII and section G). The VB

wavefunction changes from P_1/R to P_1/P_2. One sees similar change along a linear interpolation from $(syn)^{[1,2]}_{\min} CI\{C_1\}$ to $(asyn)^{[1,2]}_{scan} CI\{C_1\}$ (see Table S-IX and section G), confirming the qualitative picture in Figure 4.

Summary of computational results of the transition-structure region on S_1 potential energy surface: We now proceed with the computational documentation of the various reaction S_1 pathways. The relative energies and geometries of the important points (Fig. 1 and 2) of the transition structure region of the S_1 potential surface are given in Table II. The characterization of the transition states which are encountered initially on S_1: $(syn)^{[1,2]}_{TS} S_1\{C_s\}$, $(syn)^{[1,3]}_{TS} S_1\{C_s\}$, $(asyn)^{[1,2]}_{TS} S_1\{C_1\}$, $(asyn)^{[1,3]}_{TS} S_1\{C_1\}$, and $(asyn)^{[1,X]}_{TS} S_1\{C_s\}$ are given in Figure 10. In each case the transition vector clearly involves synchronous or asynchronous bond formation.

Table II. Characterization of the stationary points on the S_1 PES. See section A of supporting information for geometries, frequencies and animations. See also Table S-I in supporting information for CASPT2 results and energies in Hartree.

Point	ΔE[a] (kcal/mol)	Distance[b] (Å)
$(syn)^{[1,2]}_{TS} S_1\{C_s\}$	12.26	2.14/2.14
$(syn)^{[1,2]}_{sp2} S_1\{C_s\}$	25.70	2.39/2.39
$(syn)^{[1,2]}_{sp3} S_1\{C_1\}$	27.80	2.50/2.53
$(syn)^{[1,3]}_{TS} S_1\{C_s\}$	17.58	2.43/2.43
$(asyn)^{[1,2]}_{TS} S_1\{C_1\}$	11.53	1.88/2.38
$(asyn)^{[1,3]}_{TS} S_1\{C_1\}$	1.86	1.58/3.05
$(asyn)^{[1,3]}_{sp2} S_1\{C_1\}$	18.64	2.14/2.92
$(syn)^{[1,4]}_{sp3} S_1\{C_{2v}\}$	32.50	2.54/2.54
$(asyn)^{[1,X]}_{\min} S_1\{C_s\}$	0.49	1.59/3.12 (ortho); 3.93 (meta); 4.26 (para)
$(asyn)^{[1,X]}_{TS} S_1\{C_s\}$	16.81	2.10/3.36 (ortho); 3.79 (meta); 3.98 (para)

[a] Relative to the S_1 energy of benzene + ethylene at S_0 geometries and at a distance of 10 Å.
[b] Distance between the two pairs of reactive carbon atoms in ethylene and benzene.

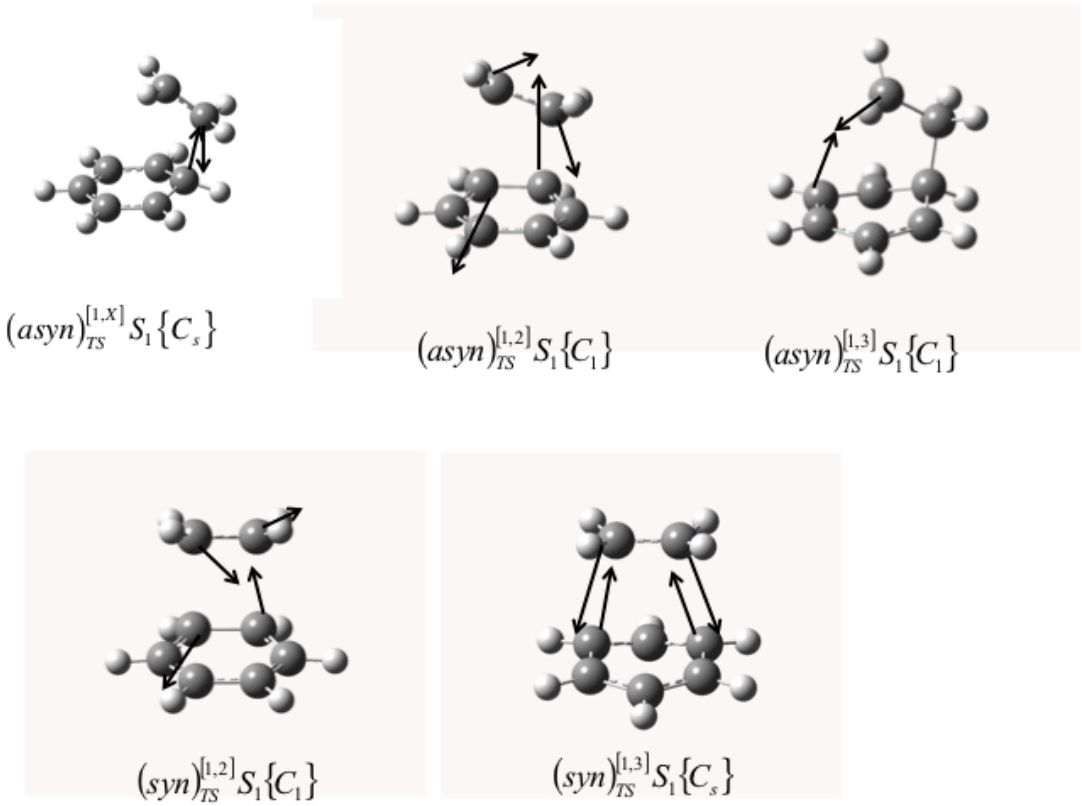

Figure 10. Normal modes associated with imaginary frequencies of the transition states (see table I for C-C distances) found on S_1. For animations and further details see supporting information Section A and Table S-I

The points with more than one imaginary frequency such as $(syn)_{sp2}^{[1,2]} S_1\{C_s\}$ or $(asyn)_{sp2}^{[1,3]} S_1\{C_1\}$ were computed just to confirm the shape of the potential surfaces. (See Table S-V in supporting information for further details and animations). We have run SDP from the sp2 points and the results are indicated in Figures 1 and 2 with dotted lines with arrows. We can see that from $(syn)_{sp2}^{[1,2]} S_1\{C_s\}$ there are SDP to $(syn)_{TS}^{[1,2]} S_1\{C_s\}$ and the reactants, and to the two equivalent $(asyn)_{TS}^{[1,X]} S_1\{C_s\}$ structures. Thus $(syn)_{sp2}^{[1,2]} S_1\{C_s\}$ is a local "mountain top" dividing the reaction valleys.

The results for the [1,2] reaction path are surprising at first sight. While the conical intersection point $(syn)_{\min}^{[1,2]} CI\{C_1\}$ is similar to the 2+2 intersection of two ethylenes, the obvious candidate for a TS connecting the reactants would have been a structure similar to $(syn)_{sp2}^{[1,2]} S_1\{C_s\}$, but this turns out to be a second order saddle point. There is an additional transition state $(syn)_{TS}^{[1,2]} S_1\{C_s\}$; but this connects two equivalent $(syn)_{\min}^{[1,2]} CI\{C_1\}$ structures. So the $(syn)_{\min}^{[1,2]} CI\{C_1\}$ conical intersection is reached from $(asyn)_{\min}^{[1,X]} S_1\{C_s\}$

via a transition state $(asyn)_{TS}^{[1,2]} S_1\{C_1\}$ shown in Figure 10. This connectivity (see Figure 1 & 2) has been confirmed by MEP in both directions (See Table S-V and section F). Thus the [1,2] paths starts as an asynchronous path but becomes synchronous as it passes through the conical intersection. This is in marked contrast to the [1,3] case which we will now discuss.

For the [1,3] regioselectivity, both a synchronous [1,3] path: $(syn)_{TS}^{[1,3]} S_1\{C_1\}$ to $(syn)_{TS}^{[1,3]} CI\{C_s\}$ and an asynchronous [1,3] path, $(asyn)_{TS}^{[1,X]} S_1\{C_s\}$ to $(asyn)_{\min}^{[1,X]} S_1\{C_s\}$, to $(asyn)_{TS}^{[1,3]} S_1\{C_1\}$ and finally to $(asyn)_{\min}^{[1,3]} CI\{C_1\}$ exist. All the details have been confirmed with MEP (See Table S-V and section F in supporting information). The $(asyn)_{sp2}^{[1,3]} S_1\{C_1\}$ structure is a "mountain top" separating these two valleys. SDP then connect the sp2 with reactants and $(asyn)_{\min}^{[1,3]} CI\{C_1\}$ in one direction and $(syn)_{TS}^{[1,3]} S_1\{C_1\}$ with $(asyn)_{TS}^{[1,X]} S_1\{C_s\}$ in the other (see animations and Table S-I, as well as SDP in Table S-V).

We have not been able to locate a direct 1,4 synchronous path. The only synchronous [1,4] point we have found is a C_{2v} structure ($(syn)_{sp3}^{[1,4]} S_1\{C_{2v}\}$), which is a 3rd-order saddle point, which lies too high in energy to be important mechanistically. (see Table II and Table S-I). As discussed previously, there is an asynchronous [1,4] reaction path (constrained to C_s symmetry) from the biradical minimum $(asyn)_{\min}^{[1,X]} S_1\{C_s\}$, however this path lies along a ridge (See section E in supporting information for further details.)

From the preceding analysis is clear that there are four key TS which are important on the way from reactants to the seam: two rate determining $(asyn)_{TS}^{[1,X]} S_1\{C_1\}$ and $(syn)_{TS}^{[1,3]} S_1\{C_s\}$, and two from the biradical minimum $(asyn)_{TS}^{[1,2]} S_1\{C_1\}$ and $(asyn)_{TS}^{[1,3]} S_1\{C_1\}$. So there are 3 possible reaction paths to the seam, identified as paths 1-3 at the end of the previous sub-section.

Summary of computational results for the S_0 Reaction pathways from the conical intersection seams: We have optimized several conformations and isomers of ground state products as well as biradical intermediates on S_0. The results are summarized in table IV.

Table IV. S_0 optimized geometries in the product side. See section A in supporting information for further details as well as Table S-III.

Point	ΔE^a (kcal/mol)	Distance[b] (Å)
$(asyn)_{\min}^{[1,X]} S_0\{C_s\}$	-55.38	1.62/3.16 (ortho); 3.76 (meta); 4.01 (para)

$(asyn)_{TS}^{[1,2]}S_0\{C_1\}$	-49.21	1.57/2.49
$(asyn)_{TS}^{[1,3]}S_0\{C_1\}$	-22.68	1.61/2.08
$(asyn)_{TS}^{[1,4]}S_0\{C_s\}$	-61.07	2.14/2.14
[1,2]-adduct$_1$	-93.08	1.58/1.58
[1,2]-adduct$_2$[c]	-92.51	1.59/1.59
[1,3]-adduct$_1$[d]	-47.20	1.59/1.59
[1,3]-adduct$_2$	-85.94	1.55/1.57
[1,4]-adduct	-98.82	1.59/1.59

[a] Relative to the S_1 energy of benzene + ethylene at S_0 geometries and at a distance of 10 Å. [b] Distance between the two pairs of reactive carbon atoms in ethylene and benzene. [c]Structure which is almost the same as [1,2]-adduct$_1$. [d] Minimum but with a very low positive frequency, clearly a precursor of the other meta minimum.

The reaction path from the point where the excited state reaction path passes through the conical intersection on its way to products (table IV) is not well defined. We have previously used the concept of an initial reaction direction (IRD) to provide an initial search direction for an MEP computation[38,39], as discussed previously, this has not worked very well in this problem. Accordingly we have used SDP to define a qualitative reaction path. The SDP will terminate at a product or reactant like structure if the step size is sufficiently small.

We have been able to generate SDP from all the CI points as shown by the dotted lines with arrows in Figures 1 and 2. We discuss only a few examples (all the results are collected in sup info (see Table S-V and sections F-I). We have found MEP and SDP that terminate in the product region from and $(syn)_{TS}^{[1,3]}CI\{C_s\}$. In the reverse direction, for $(syn)_{\min}^{[1,2]}CI\{C_1\}$, the distance benzene-ethylene increases (i.e. reactants are formed again). In this case, in the MEP, we followed the DC vector from $(syn)_{\min}^{[1,2]}CI\{C_1\}$, and the GD vector from $(syn)_{TS}^{[1,3]}CI\{C_s\}$.

For the asynchronous CI structures only SDP could be computed. From the lowest-lying CI $(asyn)_{\min}^{[1,3]}CI\{C_1\}$ we found SDP that converged to the [1,3] product in one direction, and to the S_0 biradical minimum in the other direction. From $(asyn)_{scan}^{[1,2]}CI\{C_1\}$ also converged to 1,3 adduct. Both MEP and SDP from $(syn)_{\min}^{[1,2]}CI\{C_1\}$ converge to a 1,2 adduct..

IV Conclusions

In the photocycloaddition of an arene and an alkene there are 3 possible regioselectivities (Scheme I). In this work we show that this regioselectivity is,

in part, controlled by an extended conical intersection seam and that the shape of the conical intersection seam can be understood in terms of simple VB arguments. Of course, access to the conical intersection seam is in turn determined by the shape of the S_1 potential surface.

If one ignores any structures on S_1 for the moment, then the shape and energetics (ie the low energy regions) of the asynchronous conical intersection seam, suggests that 1,2 and 1,3 will be the preferred regioselectivities with similar weight. The syn 1,4 regioselectivity seems impossible on the basis of very high energetics and the asynchronous 1,4 path is associated with a maximum on the seam. The 1,3 asynchronous CI structure $(asyn)^{[1,3]}_{\min} CI\{C_1\}$ is the lowest point on the S_1 potential surface with $(asyn)^{[1,2]}_{scan} CI\{C_1\}$ slightly higher. Thus there exists an extended low energy region of the conical intersection seam centered on $(asyn)^{[1,3]}_{\min} CI\{C_1\}$. VB analysis shows that the pairs of VB structues along this asynchronous seam are the same and thus the shape will be determined mainly by steric effects. The synchronous [1,2] conical intersection point is much higher in energy.

On S_1 there are two overlapping mechanistic pathways corresponding to transition states between the reactants and the conical intersection seam. This topology yields three paths: i) a mixed asynchronous/synchronous [1,2] path: $(asyn)^{[1,X]}_{TS} S_1\{C_s\}$, $(asyn)^{[1,X]}_{\min} S_1\{C_s\}$, $(asyn)^{[1,2]}_{TS} S_1\{C_1\}$ to $(syn)^{[1,2]}_{\min} CI\{C_1\}$ ii) an asynchronous [1,3] path $(asyn)^{[1,X]}_{TS} S_1\{C_s\}$, $(asyn)^{[1,X]}_{\min} S_1\{C_s\}$, $(asyn)^{[1,3]}_{TS} S_1\{C_1\}$ and finally $(\mathrm{asyn})^{[1,3]}_{\min} CI\{C_1\}$ and 3) a synchronous [1,3] path: $(syn)^{[1,3]}_{TS} S_1\{C_s\}$ to $(syn)^{[1,3]}_{TS} CI\{C_s\}$. The S_1 activation energies are somewhat uncertain (CASSCF yields positive values while CASPT2 yields negative values). So the barriers may, in fact, be small which is consistent with the lack of experimental wavelength dependence. Thus role of the shape of S_1 potential surface in determining what regions of the extended seam may not be critical. Here dynamics studies may be the way ahead.

V **Acknowledgements**
J.J. Serrano-Perez is grateful for support from the European Research Council under the European Community's Seventh Framework Programme (FP7/2007-2013) / ERC grant agreement nº 251955. F.D.V. wishes to acknowledge the Research Foundation-Flanders (FWO) for a post-doctoral fellowship. F.D.P. wishes to acknowledge the FWO and the Free University of Brussels for continuous support to his research group.

Supporting Information Available: Geometries and vectors (with reference to animations) of all the stationary and relevant non-stationary points on S_1, S_0 and S_1/S_0 seam, Figures and tables which provide extra evidence and information to the main paper, discussion of the paths from S_1 to the seam via asynchronous ortho and para structures, details of the MEP/SDP paths on S_1, S_0 and S_1/S_0 seam, as well as those pathways which go back to the reactants. This material is available free of charge via the Internet at http://pubs.acs.org.

References

(1) Bearpark, M. J.; Robb, M. A. In *Reviews of Reactive Intermediate Chemistry*; John Wiley & Sons, Inc.: 2006, p 379.
(2) Bernardi, F.; Olivucci, M.; Robb, M. A. *Pure and Applied Chemistry* **1995**, *67*, 17.
(3) Bernardi, F.; Olivucci, M.; Robb, M. A. *Chem Soc Rev* **1996**, *25*, 321.
(4) Klessinger, M. *Angewandte Chemie International Edition in English* **1995**, *34*, 549.
(5) Martinez, T. J. *Nature* **2010**, *467*, 412.
(6) Robb, M. A.; Bernardi, F.; Olivucci, M. *Pure and Applied Chemistry* **1995**, *67*, 783.
(7) Serrano-Andrés, L.; Merchán, M. In *Encyclopedia of Computational Chemistry*; John Wiley & Sons, Ltd: 2004.
(8) Sicilia, F.; Bearpark, M. J.; Blancafort, L.; Robb, M. A. *Theor Chem Acc* **2007**, *118*, 241.
(9) Sicilia, F.; Blancafort, L.; Bearpark, M. J.; Robb, M. A. *J Phys Chem A* **2007**, *111*, 2182.
(10) Robb, M. A. In *Conical Intersections, Theory, Computation and Experiment*; Domcke W, Yarkony, D R, Koppel H, Eds. 2011, p 3.
(11) Streit, U.; Bochet, C. G. *Beilstein J Org Chem* **2011**, *7*, 525.
(12) Bryce-Smith, D. *Journal of the Chemical Society D: Chemical Communications* **1969**, 806.
(13) Bryce-Smith, D. *Pure and Applied Chemistry* **1973**, *34*, 193.
(14) Bryce-Smith, D.; Gilbert, A. *Tetrahedron* **1976**, *32*, 1309.
(15) Bryce-Smith, D.; Gilbert, A. *Tetrahedron* **1977**, *33*, 2459.
(16) Cornelisse, J. *Chem Rev* **1993**, *93*, 615.
(17) Houk, K. N. *Pure and Applied Chemistry* **1982**, *54*, 1633.
(18) Mattay, J. *Tetrahedron* **1985**, *41*, 2405.
(19) Mattay, J. *Angew Chem Int Edit* **2007**, *46*, 663.
(20) Mirbach, M. F.; Mirbach, M. J.; Saus, A. *Tetrahedron Lett* **1977**, 959.

(21) Neumann, F.; Jug, K. *J Phys Chem-Us* **1995**, *99*, 3511.
(22) Vanderhart, J. A.; Mulder, J. J. C.; Cornelisse, J. *J Photoch Photobio A* **1991**, *61*, 3.
(23) Bryce-Smith, D.; Foulger, B. E.; Gilbert, A. *J Chem Soc Chem Comm* **1972**, 769.
(24) Berridge, J. C.; Forrester, J.; Foulger, B. E.; Gilbert, A. *J Chem Soc Perk T 1* **1980**, 2425.
(25) Berridge, J. C.; Gilbert, A.; Taylor, G. N. *J Chem Soc Perk T 1* **1980**, 2174.
(26) Morikawa, A.; Brownste.S; Cvetanov.Rj *J Am Chem Soc* **1970**, *92*, 1471.
(27) Wilzbach, K. E.; Kaplan, L. *J Am Chem Soc* **1966**, *88*, 2066.
(28) Wilzbach, K. E.; Kaplan, L. *J Am Chem Soc* **1971**, *93*, 2073.
(29) Clifford, S.; Bearpark, M. J.; Bernardi, F.; Olivucci, M.; Robb, M. A.; Smith, B. R. *J Am Chem Soc* **1996**, *118*, 7353.
(30) Gilbert, A.; Yianni, P. *Tetrahedron* **1981**, *37*, 3275.
(31) Mattay, J. *J Photochem* **1987**, *37*, 167.
(32) Stehouwer, A. M.; Vanderhart, J. A.; Mulder, J. J. C.; Cornelisse, J. *Theochem-J Mol Struc* **1992**, *92*, 333.
(33) Vanderhart, J. A.; Mulder, J. J. C.; Cornelisse, J. *J Photoch Photobio A* **1995**, *86*, 141.
(34) Palmer, I. J.; Ragazos, I. N.; Bernardi, F.; Olivucci, M.; Robb, M. A. *J Am Chem Soc* **1993**, *115*, 673.
(35) Worth, G. A.; Robb, M. A.; Lasorne, B. *Mol Phys* **2008**, *106*, 2077.
(36) Mendive-Tapia, D.; Lasorne, B.; Worth, G. A.; Bearpark, M. J.; Robb, M. A. *Phys Chem Chem Phys* **2010**, *12*, 15725.
(37) Lasorne, B.; Worth, G. A.; Robb, M. A. *Wiley Interdisciplinary Reviews: Computational Molecular Science* **2011**, *1*, 460.
(38) Celani, P.; Robb, M. A.; Garavelli, M.; Bernardi, F.; Olivucci, M. *Chem Phys Lett* **1995**, *243*, 1.
(39) Garavelli, M.; Celani, P.; Fato, M.; Bearpark, M. J.; Smith, B. R.; Olivucci, M.; Robb, M. A. *J Phys Chem A* **1997**, *101*, 2023.
(40) Li, Q. S.; Mendive-Tapia, D.; Paterson, M. J.; Migani, A.; Bearpark, M. J.; Robb, M. A.; Blancafort, L. *Chem Phys* **2010**, *377*, 60.
(41) Bernardi, F.; Olivucci, M.; Robb, M. A.; Tonachini, G. *J Am Chem Soc* **1992**, *114*, 5805.
(42) Bearpark, M. J.; Deumal, M.; Robb, M. A.; Vreven, T.; Yamamoto, N.; Olivucci, M.; Bernardi, F. *J Am Chem Soc* **1997**, *119*, 709.
(43) Vanni, S.; Garavelli, M.; Robb, M. A. *Chem Phys* **2008**, *347*, 46.
(44) Frisch, M. J.; Trucks, G. W.; Schlegel, H. B.; Scuseria, G. E.; Robb, M. A.; Cheeseman, J. R.; Scalmani, G.; Barone, V.; Mennucci, B.; Petersson, G. A.; Nakatsuji, H.; Caricato, M.; Li, X.; Hratchian, H. P.; Izmaylov, A. F.; Bloino, J.; Zheng, G.; Sonnenberg, J. L.; Hada, M.; Ehara, M.; Toyota, K.; Fukuda, R.; Hasegawa, J.; Ishida, M.; Nakajima, T.; Honda, Y.; Kitao, O.; Nakai, H.; Vreven, T.; J. A. Montgomery, J.; Peralta, J. E.; Ogliaro, F.; Bearpark, M.; Heyd, J. J.; Brothers, E.; Kudin, K. N.; Staroverov, V. N.; Kobayashi, R.; Normand, J.; Raghavachari, K.; Rendell, A.; Burant, J. C.; Iyengar, S. S.; Tomasi, J.; Cossi, M.; Rega, N.; Millam, J. M.; Klene, M.; Knox, J. E.; J. B. Cross; Bakken, V.; Adamo, C.; Jaramillo, J.; Gomperts, R.; Stratmann, R. E.; Yazyev, O.; Austin, A. J.; Cammi, R.; Pomelli, C.; Ochterski, J. W.; Martin, R. L.; Morokuma, K.; Zakrzewski, V. G.; G. A. Voth;

Salvador, P.; Dannenberg, J. J.; Dapprich, S.; Parandekar, P. V.; Mayhall, N. J.; Daniels, A. D.; Farkas, O.; Foresman, J. B.; Ortiz, J. V.; Cioslowski, J.; Fox, D. J.; Gaussian, Inc., Wallingford CT, 2009: 2010.

(45) Merchán, M.; Serrano-Andrés, L. In *Theoretical and Computational Chemistry*; Olivucci, M., Ed.; Elsevier: 2005; Vol. Volume 16, p 35.

(46) Serrano-Andres, L.; Merchan, M. *J Mol Struc-Theochem* **2005**, *729*, 99.

(47) Aquilante, F.; De Vico, L.; Ferre, N.; Ghigo, G.; Malmqvist, P. A.; Neograd y, P.; Pedersen, T. B.; Pitonak, M.; Reiher, M.; Roos, B. O.; Serrano-Andres, L.; Urban, M.; Veryazov, V.; Lindh, R. *J Comput Chem* **2010**, *31*, 224.

(48) Sicilia, F.; Blancafort, L.; Bearpark, M. J.; Robb, M. A. *J Chem Theory Comput* **2008**, *4*, 257.

(49) Gonzalez, C.; Schlegel, H. B. *J Chem Phys* **1989**, *90*, 2154.

(50) Gonzalez, C.; Schlegel, H. B. *J Phys Chem-Us* **1990**, *94*, 5523.

(51) Atchity, G. J.; Xantheas, S. S.; Ruedenberg, K. *J Chem Phys* **1991**, *95*, 1862.

(52) Bernardi, F.; Olivucci, M.; Robb, M. A. *J Am Chem Soc* **1992**, *114*, 1606.

(53) Blancafort, L.; Celani, P.; Bearpark, M. J.; Robb, M. A. *Theor Chem Acc* **2003**, *110*, 92.

(54) Blancafort, L.; Robb, M. A. *J Phys Chem A* **2004**, *108*, 10609.

(55) Coe, J. D.; Martinez, T. J. *J Am Chem Soc* **2005**, *127*, 4560.

(56) Coe, J. D.; Martinez, T. J. *J Phys Chem A* **2006**, *110*, 618.

(57) Bernardi, F.; De, S.; Olivucci, M.; Robb, M. A. *J Am Chem Soc* **1990**, *112*, 1737.

(58) Boggio-Pasqua, M.; Groenhof, G.; Schafer, L. V.; Grubmuller, H.; Robb, M. A. *J Am Chem Soc* **2007**, *129*, 10996.

(59) Bernardi, F.; Olivucci, M.; Robb, M. A. *Accounts Chem Res* **1990**, *23*, 405.